Pediatr Radiol (2005) 35: 396–401
DOI 10.1007/s00247-004-1376-4

ORIGINAL ARTICLE

Gerald F. Greil
Ulrich Kramer
Florian Dammann
Fritz Schick
Stephan Miller
Claus D. Claussen
Ludger Sieverding

Diagnosis of vascular rings and slings using an interleaved 3D double-slab FISP MR angiography technique

Received: 16 September 2004
Accepted: 21 October 2004
Published online: 5 January 2005

Electronic supplementary material is available for this article at http://dx.doi.org/10.1007/s00247-004-1376-4

G. F. Greil (✉) · L. Sieverding
Department of Paediatric Cardiology, Children's Hospital, University of Tuebingen, Hoppe Seyler Strasse 3, 72076 Tuebingen, Germany
E-mail: gerald.greil@med.uni-tuebingen.de
Tel.: +49-7071-2987147
Fax: +49-7071-295127

U. Kramer · F. Dammann · F. Schick
S. Miller · C. D. Claussen
Department of Diagnostic Radiology, University of Tuebingen, Tuebingen, Germany

Abstract ***Background***: Congenital upper airway obstruction and dysphagia may be caused by vascular rings and slings. Often, invasive and radiation-dependent diagnostic procedures are needed to clarify the diagnosis. ***Objective***: To evaluate the diagnostic utility of high-resolution, free-breathing three-dimensional double-slab fast imaging with steady precession magnetic resonance angiography (3D FISP MRA) in infants and children with respiratory upper airway obstruction and/or dysphagia for detection or exclusion of vascular rings and slings. ***Materials and methods***: Eleven patients (median age 1.3 years; range 5.1 months to 15.8 years) were investigated prospectively with 3D FISP MRA and spin-echo techniques. Additional diagnostic data were available from surgery ($n=7$), cardiac catheterization ($n=5$), CT ($n=2$), barium swallow ($n=3$) and bronchoscopy/oesophagoscopy ($n=4$). ***Results***: In one case, diagnosis was missed with low-resolution spin-echo sequences, but high-resolution 3D FISP MRA revealed a double aortic arch. 3D FISP MRA accurately found ($n=8$) or excluded ($n=3$) vascular rings or slings in all patients. Using a five-level grading system for 3D FISP MRA image quality (1 = non-diagnostic; 5 = excellent), the mean grade was 4.3 ± 0.7 with no significant grade difference between two independent observers ($P=0.81$). ***Conclusions***: High-resolution 3D FISP MRA accurately defined or excluded vascular rings and slings in patients with respiratory symptoms and/or dysphagia. This technique may provide a non-invasive, radiation-free alternative without contrast agents for diagnosis of vascular rings and slings in free-breathing infants and children.

Keywords Congenital heart disease · Vascular rings and slings · MRI · FISP MRA

Introduction

Respiratory distress and dysphagia are common symptoms in paediatric patients [1]. Vascular rings and slings are possible causes of these symptoms which can be treated by vascular surgery [2]. Historically, invasive or radiation-dependent procedures have been used for diagnosis [3–5]. ECHO is a non-invasive diagnostic procedure, but is limited by acoustic windows [6]. Oesophagoscopy/bronchoscopy is an invasive procedure and vascular anatomy cannot be assessed accurately for surgical treatment [1, 4, 7]. CT leads to radiation exposure and iodinated contrast agents are needed. For CT and contrast-enhanced magnetic resonance angiography (MRA), breath holding is needed for sufficient vascular imaging, which is particularly difficult in infants and children [8, 9]. Cardiac catheterization is an expensive procedure that carries risks associated with its invasive nature, ionizing radiation exposure and use of iodinated contrast agents [10]. Therefore, there is a need for a

reliable, non-invasive and radiation-free technique applicable particularly to infants and children.

High-resolution, three-dimensional, double-slab fast imaging with steady precession MRA (3D FISP MRA) is a free-breathing, non-invasive technique without contrast agents for delineation of vascular and non-vascular structures within the thorax. With this prospective study, the clinical utility of this technique was evaluated for the diagnosis of vascular rings and slings. Spin-echo and other MR techniques, cardiac catheterization, surgery, CT, barium swallow and bronchoscopy/oesophagoscopy were used for comparison.

Materials and methods

Patients

Eleven patients (median age 1.3 years; range 5.1 months to 15.8 years; weight 5.0–75 kg; 7 boys, 4 girls) with respiratory symptoms of unclear origin and/or dysphagia were included in this prospective study. The indication for MRI was a failure of ECHO to establish a diagnosis or the necessity for clear delineation of the vascular anatomy and its spatial relationship to non-vascular structures prior to surgery.

Based on the theoretical double-arch model originally introduced by Edwards [11], the vascular rings and slings in this study were classified according to Kussman et al. [7] as follows:

1. Double aortic arch
2. Right aortic arch
   a. Aberrant left subclavian artery with left ligamentum arteriosum
   b. Mirror-image branching with right (retro-oesophageal) ligamentum arteriosum
3. Left aortic arch
   a. Aberrant right subclavian artery
   b. Right descending aorta and right ligamentum arteriosum
4. Anomalous innominate artery
5. Cervical aortic arch
6. Pulmonary artery sling

Written informed consent for MRI was obtained from all legal guardians of the participants, and the protocol was approved by the local Ethics Committee on Clinical Investigation.

MRI protocol

No contraindication to MRI existed in any of the referred patients. All studies were performed on a commercial 1.5-T whole-body MR unit (Magnetom Vision, Siemens AG, Germany; software version VB 33G, gradient system 25 mT/m, rise time 25μs/mT/m). Children below 20 kg body weight were examined with the circulatory polarized head coil of the manufacturer ($n=7$). The body phased-array coil was used for children and adolescents weighing more than 20 kg body weight ($n=4$). No contrast agents were used in any of the patients. Patients younger than 10 years were sedated orally with chloral hydrate 100 mg/kg body weight and 0.1 mg/kg body weight midazolam.

High-resolution 3D FISP MRA

High-resolution 3D FISP MRA was performed on all 11 patients (Table 1). This technique has been previously described [12]. Briefly, the technique uses simultaneous recording of two thin 3D slabs (each with a thickness of approximately 12 mm) with a gap of at least 30 mm between the slabs, allowing coverage of a relatively large volume per measuring time without marked suppression of flowing spins. Several measurements with shifted slabs are necessary to cover a large volume of interest with contiguous slices. The structure of the developed double-slab technique is based on an ECG-triggered flow-compensated 3D FISP sequence [13]. The loop structure is similar to magnetization-prepared rapid gradient-echo (MP-RAGE) imaging [12]. This means that in each RR interval, all phase-encoding steps in the slice direction of both slabs are recorded during each diastole.

The sequence allows a maximum resolution in the read and phase directions of 0.78 mm corresponding to a 256×256 matrix and 200 mm field of view (Table 1). In the third dimension the best possible resolution is 1 mm [12]. The sequence is flow compensated in the read and slice selection direction. In spite of the long read-out

Table 1 MRI acquisition parameters

Technique	T1-weighted spin-echo	3D FISP MRA
Flip angle	90°–180°	17°–25°
Imaging plane	Transverse	Transverse ($n=8$) Sagittal ($n=3$) Coronal ($n=1$)[a]
Matrix (pixels)	256×256	256×256
Field of view (mm)	Min.: 200 Max.: 340	Min.: 200 Max.: 260
TR (ms)	530 ± 200 (350–910)	12.5
TE (ms)	12	5.5
Slice alignment	Contiguous	Contiguous
Slice thickness (mm)	2 ($n=6$) 3 ($n=4$) 4 ($n=1$)	1.25 ($n=11$)

FISP fast imaging with steady precession
[a] One patient had coronal and sagittal image acquisition

Table 2 Diagnoses and diagnostic procedures

No.	Diagnosis	Associated CHD	Surgery	Angiography
1	Double aortic arch	None	Yes	Yes
2	Double aortic arch	None	Yes	No
3	Right aortic arch with aberrant left subclavian artery with left ligamentum arteriosum	None	Yes	No
4	Right aortic arch with aberrant left subclavian artery with left ligamentum arteriosum	None	Yes	Yes
5	Right aortic arch with mirror-image branching with right (retro-oesophageal) ligamentum arteriosum	None	Yes	Yes
6	Left aortic arch with aberrant right subclavian artery	LSVC, truncus bicaroticus	No	No
7	Left aortic arch with aberrant right subclavian artery	PFO, VSD, dysplastic TV	Yes	Yes
8	Pulmonary artery sling	PFO	No	No
9	Exclusion of an arterial ring or sling	None	No	No
10	Exclusion of an arterial ring or sling	CoA, VSD	Yes	Yes
11	Exclusion of an arterial ring or sling	None	No	No

CHD congenital heart disease, *CoA* coarctation of the aorta, *LSVC* left superior vena cava, *PFO* persistent foramen ovale, *TV* tricuspid valve, *VSD* ventricular septal defect

interval, the sequence has a short echo time (TE) of 5.5 ms and a repetition time (TR) of only 12.5 ms. The flip angle was chosen between 17 ° and 25 ° (Table 1).

All examinations were performed using uncoached free breathing. With ECG triggering, data were acquired in mid-diastole to minimize flow artefacts or blurring of the image due to fast heart movements. The scanning protocol was accomplished in approximately 12–15 min.

Other MRI techniques

Spin-echo sequences were used in all 11 patients (Table 1). 2D cine fast low-angle shot (FLASH) and velocity-encoded imaging were also applied for vascular imaging.

Conventional angiography

All patients were sedated with IV ketamine and midazolam during catheterization. Several contrast agent injections in the aorta were recorded with biplane fluoroscopy for later review.

Other investigations

Chest radiographs and ECHO were obtained in all patients. Cardiac catheterization and surgery were used as reference standards when available (Table 2). Additionally, CT, barium swallow and bronchoscopy/oesophagoscopy were used for comparison.

Data analysis

The 3D FISP MRA diagnoses were compared with all other available diagnostic information for discrepancies. High-resolution 3D FISP MRA data were reviewed offline by a paediatric cardiologist and a radiologist specialized in cardiac MRI using a combination of the following techniques: user-defined subvolume maximal intensity projection (MIP), multiplanar reformatting (MPR) and 3D volume rendering. MIP and MPR were performed on a Siemens workstation (Leonardo, Siemens AG, Germany); 3D volume rendering on a Vitrea 2 workstation (Vital Images Corporation, Plymouth, MN, USA). Using these viewing techniques, the aorta and its major branches, the trachea and the oesophagus were examined in detail.

An interobserver evaluation of the image quality of 3D FISP MRA images was performed by two of the authors (G.F.G., L.S.). A modified five-level scoring

Table 3 Scoring system for evaluation of image quality (modified from [14])

	Score value
Aortic arch, great vessels, trachea and oesophagus not visible (no diagnostic information)	1
Aortic arch, great vessels, trachea and oesophagus visible with markedly blurred borders, and/or connections, and/or anatomic course (poor quality diagnostic information; diagnosis is questionable)	2
Aortic arch, great vessels, trachea and oesophagus visible with moderately blurred borders, and/or connections, and/or anatomic course (moderate quality diagnostic information but able to establish diagnosis)	3
Aortic arch, great vessels, trachea and oesophagus visible with mildly blurred borders, and/or connections, and/or anatomic course (good quality diagnostic information with definite diagnosis)	4
Aortic arch, great vessels, trachea and oesophagus visible with sharply defined borders, connections, and anatomic course (excellent quality diagnostic information)	5

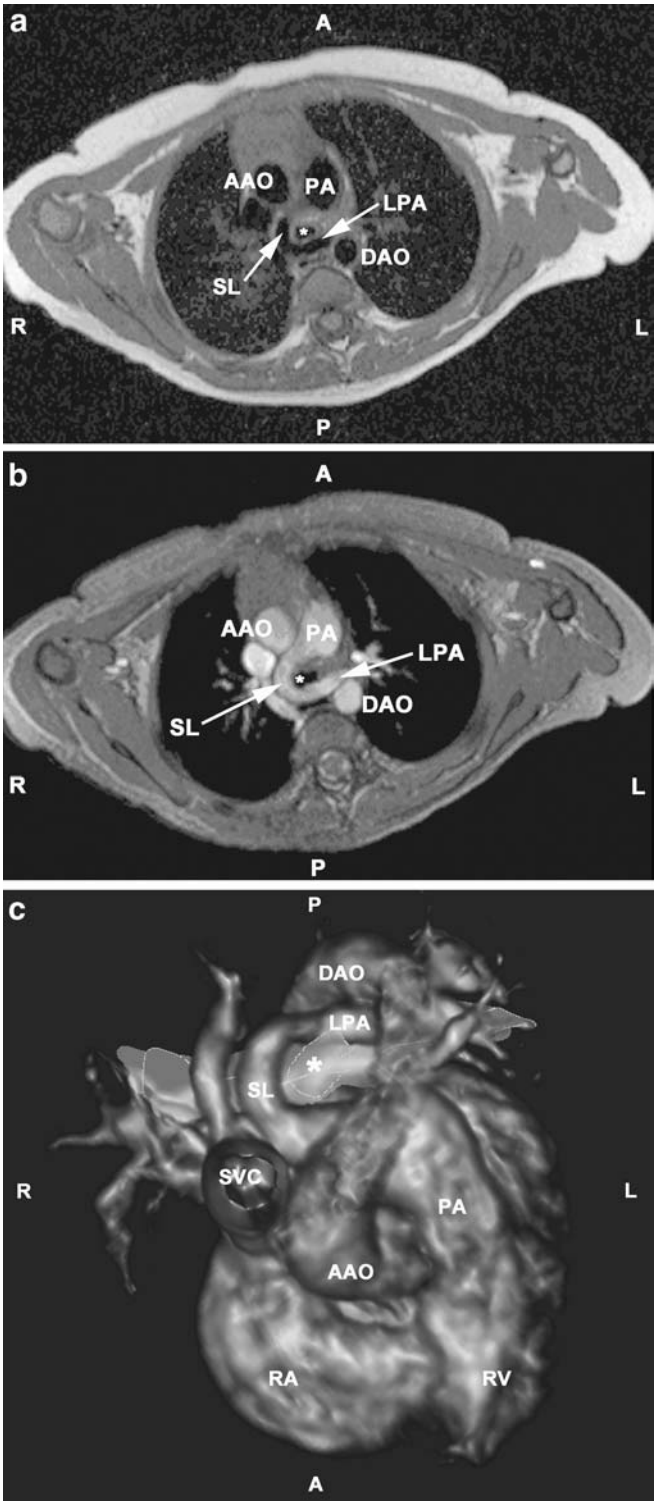

◀

Fig. 1 A 2-year-old patient. **a** Axial T1-weighted spin-echo image (2-mm slice thickness) shows a pulmonary artery sling of the left pulmonary artery. **b** Angulated MIP of the pulmonary artery sling (3D FISP MRA). **c** A 3D volume-rendered model based on a 3D FISP MRA dataset. The tracheo-bronchial tree is coloured *blue*. (*A* anterior, *P* posterior, *L* left, *R* right, *LPA* left pulmonary artery, *AAO* ascending aorta, *DAO* descending aorta, *PA* pulmonary artery, *SL* pulmonary artery sling, *RA* right atrium, *RV* right ventricle, *SVC* superior vena cava, *asterisks* trachea)

system [14] was used, ranging from 1, when the aortic arch structures, trachea and oesophagus were not visible, to 5, when these structures were visible with sharply defined borders (Table 3). Diagnosis could be established with a scoring level of 3 or higher.

Continuous data are reported as mean ± SD (median, range). The agreement between observers regarding image quality was assessed by the Wilcoxon signed rank test. $P < 0.05$ was considered significant.

Results

Median time from first symptoms to diagnosis in our MR unit was 7.3 months with a range from 2.9 months up to 15.7 years. All MRI studies were technically successful without adverse effects. 3D FISP MRA data were acquired within 12–15 min covering the neck and upper thorax. Both examiners were blinded to the results. MIP or MPR images were constructed nearly instantaneously (Fig. 1). 3D volume-rendered models (Fig. 1) were created to demonstrate the spatial relationship between vascular and non-vascular intrathoracic structures in all three dimensions. 3D FISP MRA clearly demonstrated the origin, course and connections of the aorta and its branches as well as the trachea and the oesophagus. The spatial relationship between vascular and non-vascular structures was clearly delineated. Final diagnosis was established in all patients independently by two experienced examiners (G.F.G., U.K.) using the above-described techniques. The diagnosis was confirmed by spin-echo MRI ($n = 11$), cardiac catheterization ($n = 5$) and/or operation ($n = 7$) (Table 2). Additional confirmation of diagnosis was obtained by other MRI techniques such as 2D cine FLASH ($n = 5$) and velocity-encoded imaging ($n = 2$). CT ($n = 2$); barium swallow ($n = 3$), bronchoscopy/oesophagoscopy ($n = 4$), chest radiographs ($n = 11$) and ECHO ($n = 11$) were also applied.

Table 2 summarizes the diagnoses in our patients. In patient 6 (left aortic arch with aberrant right subclavian artery) and patient 8 (pulmonary artery sling of the left pulmonary artery; Fig. 1) the vascular and non-vascular anatomy was clearly shown by 3D FISP MRA and spin-echo images. MRI results showed good correlation. With only mild clinical symptoms, no surgery has been required so far. Three patients had vascular rings excluded after ECHO had been unable to establish a final diagnosis. Beside 3D FISP MRA, spin-echo, cine FLASH and velocity-encoded imaging clearly demonstrated normal vascular and non-vascular anatomy within the thorax in patient 9. Patient 11 had a vascular

ring and sling excluded by 3D FISP MRA, spin-echo and a normal barium swallow examination. After more than 8 years of follow-up, he is symptom free. In all other patients the MRI findings were confirmed by surgery (Table 2).

At an external institution, spin-echo images (4-mm slice thickness with 1-mm spacing, matrix 256×256, FOV 300 mm) were acquired in a 5.4-year-old patient (patient 2). A vascular abnormality was not detected as a possible cause of known significant respiratory symptoms. About 1.8 years later, after more than 6 years of drug treatment for obstructive lung disease and extensive diagnostic procedures, a double aortic arch was diagnosed with 3D FISP MRA (1.25-mm slice thickness, contiguous slices, matrix 256×256, FOV 210 mm) at our institution. At operation, the diagnosis of a double aortic arch was confirmed and the small left aortic arch was divided. The patient is now free of symptoms.

Image quality

High-resolution 3D FISP MRA data were reviewed offline. Interobserver evaluation of image quality was performed by two of the authors (G.F.G., L.S.) using the five-level scoring system as defined earlier. The mean score was 4.3 ± 0.7 (median 4.0, range 3–5). Close agreement was found between the two observers, with a mean difference of 0.1 ± 0.7 (range −1.0 to 1.0; $P = 0.81$).

Discussion

Although vascular rings and slings are rare causes of respiratory symptoms in infants and children, they are important sources of airway and oesophageal obstruction [1, 3, 15]. Diagnosis may be delayed and years of clinical symptoms and drug treatment may precede final diagnosis and operative treatment [1, 16]. In our own series, diagnosis was delayed up to 15.7 years due to insufficient imaging of the vascular abnormality. Surgery gave very good results with prompt relief of clinical symptoms [3, 16–18]. This stresses the importance of a safe and reliable method for exclusion or verification of a vascular ring and sling in infants and children.

To our knowledge, this study is the largest reported series of patients with vascular rings and slings diagnosed by free-breathing 3D FISP MRA without the use of contrast agents. Usually, diagnostic procedures are invasive, leading to radiation exposure, or general anaesthesia is needed for breath holding [1, 4, 5, 7, 8, 10, 19]. Spiral CT and recently multidetector CT have been used as 3D methods to visualize vascular rings and slings with promising results [8]. However, ionizing radiation, iodinated contrast agents and general anaesthesia are needed in infants and children for breath holding [8]. As an alternative, contrast-enhanced MRA has been used as a radiation-free method [8]. However, contrast agents are needed, spatial resolution is usually lower than with 3D FISP MRA; breath holding improves image quality significantly, requiring general anaesthesia in infants and children [8, 9].

To establish the diagnosis, spatial resolution needs to be appropriate for the size of the patient. As described above, in a 5.4-year-old symptomatic patient, a double aortic arch was not detected by low-resolution, T1-weighted spin-echo images (4-mm slice thickness with 1-mm spacing) at an external institution. About 1.8 years later, high-resolution 3D FISP MRA (1.25-mm contiguous slices) accurately demonstrated a double aortic arch at our institution. Anatomy was confirmed at surgery.

Free-breathing 3D FISP MRA offers high-resolution images (minimal voxel size $0.78 \times 0.78 \times 1.0$ mm^3) of the upper thorax without contrast agents within 12–15 min [12]. Adjacent structures, such as the trachea and oesophagus are imaged within the 3D volume. MIP (Fig. 1) and 3D volume rendering (Fig. 1) depict the spatial relationship between vascular and non-vascular structures. Compared to spin-echo techniques (black blood), 3D FISP MRA (bright blood) allows better differentiation between vascular and non-vascular structures (Fig. 1). 3D FISP MRA data can be presented as volume-rendered models (Fig. 1), including movie images. This is not possible with spin-echo images. Furthermore, 3D FISP MRA offers higher spatial resolution than spin-echo (Table 1).

In our series, 3D FISP MRA accurately diagnosed or excluded vascular rings and slings in patients aged 5 months to 15.8 years. Regarding this patient population, high-resolution 3D FISP MRA proved to be a reliable tool for the detection or exclusion of vascular rings and slings in free-breathing infants and children.

Future perspectives

Parallel acquisition techniques [20, 21] may provide faster image acquisition, and promising results have been obtained in free-breathing patients using contrast agents [8, 22]. Alternatively, steady-state free precession [13] and spectrally selective fat saturation T2 pre-pulses [23] may increase contrast between blood, fat and myocardium. Combined with prospective navigator-guided breathing [24], high-resolution images of blood vessels may be obtained [25]. Techniques such as arterial spin tagging may also improve vessel contrast in free-breathing patients without the use of contrast agents [26, 27].

Limitations

The number of subjects in this study is small and further clinical study is needed. It is important to note that fi-

brous tissue such as ductal remnants cannot be imaged reliably with this technique. However, the presence of compression of the trachea and/or the oesophagus or the presence of a Kommerell diverticulum imaged with high-resolution 3D FISP MRA may lead to the correct diagnosis.

In conclusion, in patients with upper airway obstruction of unclear origin and/or dysphagia, high-resolution 3D FISP MRA reliably detects or excludes vascular rings and slings. Such an approach may provide a non-invasive radiation-free alternative when transthoracic ECHO image quality is inadequate, thereby reducing the need for invasive and radiation-dependent diagnostic procedures.

Acknowledgements We thank the "EHLKE" foundation and the "Stiftung zur Förderung der Erforschung von Zivilisationserkrankungen, Baden-Baden, Germany" for financial support and Vital Images Corporation, Plymouth, MN, USA, for technical assistance in volume rendering the 3D datasets.

References

1. Bakker DA, Berger RM, Witsenburg M, et al (1999) Vascular rings: a rare cause of common respiratory symptoms. Acta Paediatr 88:947–952
2. Gross RE (1945) Surgical relief for tracheal obstruction from a vascular ring. N Engl J Med 233:586–590
3. Sebening C, Jakob H, Tochtermann U, et al (2000) Vascular tracheobronchial compression syndromes—experience in surgical treatment and literature review. Thorac Cardiovasc Surg 48:164–174
4. Dodge-Khatami A, Tulevski II, Hitchcock JF, et al (2002) Vascular rings and pulmonary arterial sling: from respiratory collapse to surgical cure, with emphasis on judicious imaging in the hi-tech era. Cardiol Young 12:96–104
5. Berdon WE (2000) Rings, slings, and other things: vascular compression of the infant trachea updated from the midcentury to the millennium—the legacy of Robert E. Gross, MD, and Edward B. D. Neuhauser, MD. Radiology 216:624–632
6. Geva T, Kreutzer J (2001) Diagnostic pathways for evaluation of congenital heart disease. In: Crawford MH, DiMarco JP (eds) Cardiology. Mosby International, London, pp 1–22
7. Kussman BD, Geva T, McGowan FX (2004) Cardiovascular causes of airway compression. Paediatr Anaesth 14:60–74
8. Eichhorn J, Fink C, Delorme S, et al (2004) Rings, slings and other vascular abnormalities. Ultrafast computed tomography and magnetic resonance angiography in pediatric cardiology. Z Kardiol 93:201–208
9. Greil GF, Powell AJ, Gildein HP, et al (2002) Gadolinium-enhanced three-dimensional magnetic resonance angiography of pulmonary and systemic venous anomalies. J Am Coll Cardiol 39:335–341
10. Vitiello R, McCrindle BW, Nykanen D, et al (1998) Complications associated with pediatric cardiac catheterization. J Am Coll Cardiol 32: 1433–1440
11. Edwards JE (1948) Anomalies of the derivates of the aortic arch system. Med Clin North Am 52:925–949
12. Forster J, Sieverding L, Breuer J, et al (1998) High-resolution cardiac imaging using an interleaved 3D double slab technique. Magn Reson Imaging 16:1155–1162
13. Oppelt A, Graumann R, Barfuß H, et al (1986) FISP—a new fast MRI sequence. Electromedica 54:15–18
14. Danias PG, McConnell MV, Khasgiwala VC, et al (1997) Prospective navigator correction of image position for coronary MR angiography. Radiology 203:733–736
15. Park SC (1981) Symposium on pediatric otolaryngology. Vascular abnormalities. Pediatr Clin North Am 28:949–955
16. Subramanyan R, Venugopalan P, Narayan R (2003) Vascular rings: an important cause of persistent respiratory symptoms in infants and children. Indian Pediatr 40:951–957
17. Marmon LM, Bye MR, Haas JM, et al (1984) Vascular rings and slings: long-term follow-up of pulmonary function. J Pediatr Surg 19:683–692
18. Chun K, Colombani PM, Dudgeon DL, et al (1992) Diagnosis and management of congenital vascular rings: a 22-year experience. Ann Thorac Surg 53:597–602
19. Beekman RP, Hazekamp MG, Sobotka MA, et al (1998) A new diagnostic approach to vascular rings and pulmonary slings: the role of MRI. Magn Reson Imaging 16:137–145
20. Pruessmann KP, Weiger M, Boesiger P (2001) Sensitivity encoded cardiac MRI. J Cardiovasc Magn Reson 3:1–9
21. Sodickson DK, Manning WJ (1997) Simultaneous acquisition of spatial harmonics (SMASH): fast imaging with radiofrequency coil arrays. Magn Reson Med 38:591–603
22. Muthupillai R, Vick GW III, Flamm SD, et al (2003) Time-resolved contrast-enhanced magnetic resonance angiography in pediatric patients using sensitivity encoding. J Magn Reson Imaging 17:559–564
23. Brittain JH, Hu BS, Wright GA, et al (1995) Coronary angiography with magnetization-prepared T2 contrast. Magn Reson Med 33:689–696
24. McConnell MV, Khasgiwala VC, Savord BJ, et al (1997) Prospective adaptive navigator correction for breath-hold MR coronary angiography. Magn Reson Med 37:148–152
25. Sorensen TS, Korperich H, Greil GF, et al (2004) Operator-independent isotropic three-dimensional magnetic resonance imaging for morphology in congenital heart disease: a validation study. Circulation 110:163–169
26. Stuber M, Bornert P, Spuentrup E, et al (2002) Selective three-dimensional visualization of the coronary arterial lumen using arterial spin tagging. Magn Reson Med 47:322–329
27. Spuentrup E, Manning WJ, Bornert P, et al (2002) Renal arteries: navigator-gated balanced fast field-echo projection MR angiography with aortic spin labeling: initial experience. Radiology 225:589–596